An Elementary Reaction Step of the Proton Pump Is Revealed by Mutation of Tryptophan-164 to Phenylalanine in Cytochrome *c* Oxidase from *Paracoccus denitrificans*†

Camilla Ribacka,* Michael I. Verkhovsky, Ilya Belevich, Dmitry A. Bloch, Anne Puustinen, and Mårten Wikström

Helsinki Bioenergetics Group, Program for Structural Biology and Biophysics, Institute of Biotechnology, University of Helsinki, PB 65 (Viikinkaari 1), FIN-00014, Helsinki, Finland

Received June 14, 2005; Revised Manuscript Received October 3, 2005

ABSTRACT: Cytochrome *c* oxidase couples reduction of dioxygen to water to translocation of protons over the inner mitochondrial or bacterial membrane. A likely proton acceptor for pumped protons is the Δ-propionate of heme a_3, which may receive the proton via water molecules from a conserved glutamic acid (E278 in subunit I of the *Paracoccus denitrificans* enzyme) and which receives a hydrogen bond from a conserved tryptophan, W164. Here, W164 was mutated to phenylalanine (W164F) to further explore the role of the heme a_3 Δ-propionate in proton translocation. FTIR spectroscopy showed changes in vibrations possibly attributable to heme propionates, and the midpoint redox potential of heme a_3 decreased by ∼50 mV. The reaction of the oxidized W164F enzyme with hydrogen peroxide yielded substantial amounts of the intermediate **F′** even at high pH, which suggests that the mutation rearranges the local electric field in the binuclear center that controls the peroxide reaction. The steady-state proton translocation stoichiometry of the W164F enzyme dropped to ∼0.5 H^+/e^- in cells and reconstituted proteoliposomes. Time-resolved electrometric measurements showed that when the fully reduced W164F enzyme reacted with O_2, the membrane potential generated in the fast phase of this reaction was far too small to account either for full proton pumping or uptake of a substrate proton from the inside of the proteoliposomes. Time-resolved optical spectroscopy showed that this fast electrometric phase occurred with kinetics corresponding to the transition from state **A** to $\mathbf{P_R}$, whereas the subsequent transition to the **F** state was strongly delayed. This is due to a delay of reprotonation of E278 via the D-pathway, which was confirmed by observation of a slowed rate of Cu_A oxidation and which explains the small amplitude of the fast charge transfer phase. Surprisingly, the W164F mutation thus mimics a weak block of the D-pathway, which is interpreted as an effect on the side chain isomerization of E278. The fast charge translocation may be due to transfer of a proton from E278 to a "pump site" above the heme groups and is likely to occur also in wild-type enzyme, though not distinguished earlier due to the high-amplitude membrane potential formation during the $\mathbf{P_R} \rightarrow \mathbf{F}$ transition.

Cytochrome *c* oxidase is the terminal enzyme in the respiratory chain of mitochondria and many aerobic bacteria, where it catalyzes the reduction of dioxygen to water (for recent reviews, see refs *1*−*3*). The reaction is highly exergonic, and cytochrome *c* oxidase harnesses the free energy from O_2 reduction for translocation of protons over the inner mitochondrial or bacterial membrane (*4*). As a consequence, an electrochemical proton gradient is generated that can be utilized by ATP synthase or other energy-requiring reactions in the cell. The membrane embedded cytochrome *c* oxidase receives electrons, one at a time, from cytochrome *c* on the outside of the membrane (the positive, P-side). The immediate electron acceptor is the bimetallic Cu_A center from where, driven by an increase in redox potential, the electrons are transferred via heme *a* to the oxygen reducing binuclear heme a_3-Cu_B[1] center. Protons needed for water formation, as well as pumped protons, are taken up from the inner water phase (the negative, N-side) via two different pathways, named K and D after highly

† This work was supported by the Academy of Finland (project numbers 200726 and 44895), Biocentrum Helsinki, and the Sigrid Jusélius Foundation.

* To whom correspondence should be addressed at Helsinki Bioenergetics Group, Institute of Biotechnology, PB 65 (Viikinkaari 1), 00014 University of Helsinki, Finland. Phone: +358 9 19159754. Fax: +358 9 19159920. E-mail: camilla.ribacka@helsinki.fi.

[1] Abbreviations: **A**, the ferrous-oxy compound of Fe_{a3}; COMV, "mixed-valence" (two-electron reduced) enzyme ligated by carbon monoxide; ΔΨ, electric membrane potential; DM, *n*-dodecyl-β-D-maltoside; E_m, midpoint redox potental; **F**, the ferryl intermediate; **F′**, state of the binuclear a_3-Cu_B center after reacting oxidized enzyme with hydrogen peroxide (electronically equivalent to the $\mathbf{P_M}$ state); Fe_a, low-spin heme; Fe_{a3}, oxygen-binding heme; FTIR, Fourier transform infrared spectroscopy; N-side, negative side of the membrane (corresponds to the inside of the inner mitochondrial or bacterial membrane); **O**, the fully oxidized form of the enzyme; P-side, positive side of the membrane (corresponds to the outside of the inner mitochondrial or bacterial membrane); $\mathbf{P_M}$, the stable intermediate of the binuclear center detected when the "mixed-valence" enzyme reacts with O_2; $\mathbf{P_R}$, the "peroxy" intermediate of the binuclear center detected when the fully reduced enzyme reacts with O_2; **R**, the unliganded fully reduced binuclear center; τ, time constant ($t_{1/e}$); TMPD, *N*,*N*,*N*′,*N*′-tetramethyl-1,4-phenylenediamine; WT, wild-type enzyme.

10.1021/bi0511336 CCC: $30.25
Published on Web 11/22/2005

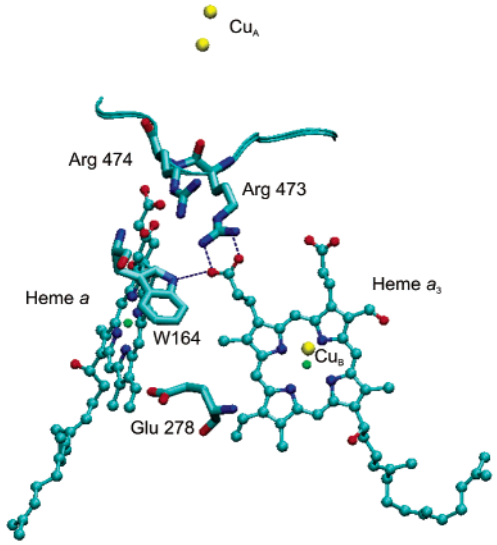

FIGURE 1: The redox-active centers of cytochrome *c* oxidase from *P. denitrificans* together with key amino acids, W164, E278, R473, and R474, discussed in this work. The Δ-propionate of heme a_3 is stabilized by hydrogen bonds from W164 and R473 and by charge interactions with R473 and R474. The figure was prepared from the *P. denitrificans* structure 1AR1 (*63*) using the Visual Molecular Dynamics software (*64*).

conserved amino acids in the respective structures (K354 and D124 in *Paracoccus denitrificans* numbering).[2] The K-pathway is important during enzyme reduction (*5*). The D-pathway is composed of water molecules stabilized by polar amino acids, through which fast proton relay can be facilitated through a Grotthuss-type mechanism. It is well established that the D-pathway has a dual function, transferring two of the four chemical and all four pumped protons. The D-pathway ends at the residue E278, which is the branching point for proton-transfer either to the binuclear center for production of water or for pumping toward the P-side of the membrane.

The nature of the first acceptor of pumped protons beyond E278, and the mechanism by which protons are delivered to this site, is still a matter of debate. An extensive hydrogen-bonded network above the hemes (*6*) is rich in water molecules and contains two well-conserved arginines, R473 and R474, apart from the heme propionates. The primary proton acceptor for the pumped proton is most likely situated in this area. However, its identity is still uncertain, and experimental studies supporting both the heme *a* and the heme a_3 Δ-propionates have been published (*7*−*9*). The Δ-propionate of heme a_3 is stabilized in its anionic state by charge interactions with R473 and R474 and by hydrogen bonds to R473 and W164 (*10*, *11*) (Figure 1). Previous studies have investigated the role of R473 and R474 in proton translocation (*7*, *12*−*16*). In this paper, we have focused on the conserved residue W164, which is hydrogen bonded to the Δ-propionate of heme a_3 via its side chain, as well as to the Δ-propionate of heme *a* via its peptide backbone (*10*). Removing the hydrogen bond to the Δ-propionate of heme a_3 by mutating W164 to phenylalanine caused relatively modest changes in the properties of the binuclear center. However, time-resolved electrometry revealed only a very small amplitude of charge translocation in the first fast phase following the reaction of the fully reduced mutant enzyme with O_2, while charge translocation during the subsequent step (**F** → **O**) had an amplitude similar to WT enzyme, despite a much slower rate. This unique phenotype is further explored, and the results may provide novel insight into the proton pump mechanism.

[2] All amino acid numbering refers to subunit I of the aa_3-type of cytochrome *c* oxidase from *Paracoccus denitrificans*.

MATERIALS AND METHODS

Enzyme Preparation. To facilitate protein purification through affinity chromatography, a six-histidine sequence has been attached to the end of the *P. denitrificans cta*DII gene, encoding subunit I of cytochrome *c* oxidase. Site-directed mutagenesis was performed as previously described (*17*), and mutations were confirmed by DNA-sequencing (ABI PRISM 310 Genetic Analyzer, Applied Biosystems) at all stages of the procedure, as well as from fermentor cultivations and cell samples from proton translocation experiments with whole cells. Bacterial growth conditions, isolation of bacterial membranes, and purification of *P. denitrificans* cytochrome aa_3 were as previously described (*17*), with the exception of the additional purification step by Ni^{2+}-NTA affinity chromatography exploiting the His-tag on the enzyme. The enzyme was eluted from the affinity column using a 5−150 mM imidazole gradient in 0.05% dodecyl maltoside (DM, Anatrace), 300 mM NaCl, and 20 mM Tris-HCl, pH 7.8. Fractions were screened on SDS−PAGE after which pure three-subunit aa_3 enzyme was concentrated and washed extensively with 20 mM Tris-HCl, pH 7.8, 0.02% DM using Amicon Ultra Centrifugal filters (Millipore).

Enzyme Activity Measurements. The steady-state oxygen reducing activity of the enzyme was measured at 25 °C with a Clark type oxygen electrode. The measuring buffer consisted of 50 mM potassium phosphate pH 6.5, 0.05% DM, supplemented with 30 μM horse heart cytochrome *c* (Sigma), 1.1 mg/mL asolectin, 0.6 mM TMPD, and 3 mM potassium ascorbate. The rate of oxygen consumption was measured after enzyme addition and for the mutants was compared to wild-type (WT) enzyme.

Proton Translocation Measurement. Proton translocation was measured both in whole cells and with isolated enzyme reconstituted into proteoliposomes. Spheroplast (whole cell) preparation and measurements were performed as previously described (*18*). Reconstitution of isolated enzyme into proteoliposomes using Bio-Beads (Bio-Rad Laboratories) is based on the method by Rigaud et al. (*19*). Proton translocation with reconstituted enzyme was measured using the oxygen pulse method described previously (*20*).

Electrometric Measurements. The time-resolved electrometric measurement is based on a method developed by Drachev and co-workers (*21*) and has been described in detail previously (*22*). In brief, proteoliposomes are attached by 10 mM $CaCl_2$ to one side of a lipid-impregnated Teflon membrane, where after Ag/AgCl electrodes situated on different sides of the membrane record the voltage generated during enzyme oxidation. The voltage sensed by the electrodes is proportional to the voltage generated over the proteoliposome membrane, which allows us to follow kinetically the charge movement over the membrane. For the pH dependence of the electrometric response, the measurements were performed in 100 mM MES, pH 6.0 and

pH 6.5, MOPS, pH 7.0, HEPES, pH 8.0, Bis-Tris propane, pH 8.5 or CHES, pH 9.0 supplemented with 100 mM glucose, 0.6 mg/mL catalase, 2.6 mg/mL glucose oxidase, and 0.5−1 μM hexaammine ruthenium [III].

Optical Backflow Measurements. The oxidized enzyme (ca. 7 μM) in 100 mM HEPES−KOH, pH 8.0, supplemented with 0.02% DM was made anaerobic on the vacuum line through repeated degassing followed by argon exchange. The sample was thereafter incubated under an anaerobic CO atmosphere and the appearance of CO-mixed valence enzyme (COMV, two-electron reduced enzyme) was detected spectrophotometrically. Electron backflow was recorded at 442 nm following CO photolysis using a single-wavelength spectrophotometer as previously described (*23*).

Time-Resolved Optical Flow-Flash. The reaction of the fully reduced W164F mutant and WT enzyme with oxygen were measured on a microsecond to millisecond time-scale by the flow-flash technique (*24*). About 15 μM enzyme in 100 mM HEPES−KOH, pH 7.4, and 0.02% DM was made anaerobic on the vacuum line, reduced with 20 mM potassium ascorbate and 5 μM TMPD, and finally incubated with 100% CO. The sample was thereafter loaded into one syringe of a stopped-flow system (RX2000, Rapid Kinetics Spectrometer Accessory, Applied Photophysics) and mixed with a 5-fold volume of oxygen-saturated buffer. The reaction was initiated by photodissociation of CO from the enzyme with a laser flash (Brilliant B, Quantel), and the kinetics of the reaction was followed optically at 445, 580, 595, and 605 nm. The measurement at 820 nm was accomplished using a light-emitting laser diode and a high-speed photo detector, with an initial enzyme concentration (before mixing 1:5) of approximately 50 μM.

Transmittance and Attenuated Total Reflection (ATR) FTIR Spectroscopy. For CO photolysis FTIR difference spectroscopy, WT and W164F mutant enzyme were diluted in 100 mM sodium phosphate in D_2O, pD 6.5, supplemented with 0.01% DM. The enzyme was made anaerobic on the vacuum line, reduced with dithionite, and mixed with CO (1 mM) after which it was loaded into the IR cell. Light-minus-dark CO difference FTIR spectra were thereafter measured as previously described (*25*). The enzyme used for ATR-FTIR spectroscopy was further purified by Source 15-Q ion exchange chromatography to remove lipid contaminants. The detergent depletion of the enzyme, which is necessary for the enzyme to form a stable protein film on top of the silicon microprism, was performed essentially as described in ref *26*. The theory behind ATR-FTIR spectroscopy and its application for cytochrome *c* oxidase from bovine heart mitochondria and *P. denitrificans* has been thoroughly explained by Rich and co-workers (*26*, *27*). The detergent-depleted enzyme was dried on top of the ATR silicon microprism surface (SensIR Technologies) by a careful flow of nitrogen until no additional changes in the absolute FTIR spectra of dried protein could be seen. The sample was thereafter rewetted with the measuring buffer, 200 mM potassium chloride and 200 mM potassium phosphate, pH 6.5 and a lid was attached on top of the sample. The lid allows for a constant flow of buffer over the sample surface (flow rate 1−2 mL/min), which makes it possible to change the condition during the experiment. The enzyme was repeatedly cycled with reductant (3 mM dithionite, anaerobic) and oxidant (1 mM ferricyanide) to get the reduced-minus-oxidized FTIR spectra (Bruker ISF 66/S spectrometer, with a liquid nitrogen-cooled MCT-A detector). An optical fiber connected to the lid covering the sample, enabled simultaneous measurement of the visible spectra (DH-2000, Mikropack, running on software from Ocean Optics Inc.).

Kinetic Measurement of the Reaction of Cytochrome c Oxidase with H_2O_2. About 15 μM of WT or W164F enzyme in 100 mM MES, pH 6.5 or CHES, pH 9.5 supplemented with 0.02% DM was reduced with 200 μM dithionite under constant nitrogen flux in one chamber of a stopped-flow apparatus (Unisoku Instruments, Kyoto, Japan). The fully reduced enzyme was thereafter mixed in a 1:1 ratio with the respective aerated buffer supplemented with 20 mM H_2O_2, which was positioned in the second chamber. Upon mixing, the oxygen in the second chamber consumes the excess dithionite and promptly oxidizes the enzyme. This experimental approach ensures immediate reoxidation of the dithionite-reduced enzyme before it is allowed to react with H_2O_2. The absorption changes were recorded with a diode array kinetic spectrophotometer (Unisoku Instruments).

Assessment of the Extent of Charge Translocation in the W164F Mutant. Oxidation of the fully reduced enzyme by O_2 is linked to the following electrogenic events, which are the sum of two phases of roughly equivalent amplitude in the WT enzyme: (i) transfer of one electron from Cu_A to the binuclear center via heme *a*, (ii) uptake of two protons from the N-side to be consumed at the binuclear center, and (iii) pumping of two protons across the membrane dielectric (*28*). If **d** is the dielectric distance between the aqueous P-side of the membrane and the heme groups (see, e.g., ref *29*), then the total charge translocation during this "oxidative phase" is **d** + 2(1-**d**) + 2, or 4-**d** charge equivalents across the membrane. The value of **d** has been estimated to be 0.32 (*29*), which yields translocation of 3.68 charge equivalents during the "oxidative phase". In contrast, the reaction with O_2 in the W164F mutant enzyme results in two electrogenic phases with widely different amplitudes, of which the first fast phase constitutes only ∼12% of the total, whereas the amplitude of the second phase is similar to that in WT enzyme (see Results). The extent of charge translocation in the first phase may be approximated by two methods. First, based on the ∼50% decrease in the proton translocation stoichiometry in the mutant, relative to WT (see Results), the overall amplitude of the "oxidative phase" should decrease by 1 charge equivalent from that in WT, i.e., to translocation of 2.68 charges, which yields translocation of 0.32 charges across the dielectric during the fast phase. Second, since the amplitude of the slow phase is similar to that in WT enzyme, i.e., 1.84 charges, the fast phase would correspond to translocation of 0.25 charges across the dielectric. Thus, both methods, based on different assumptions, suggest that the fast electrogenic phase in the mutant is due to translocation of one charge equivalent across about 30% of the dielectric.

Data Analysis. The numerical data were processed and presented using the Matlab software (The MathWorks, South Natick, MA) unless otherwise mentioned. The kinetics of the electrogenic processes were fitted with the sequential reaction model described in ref *22*. Decomposition of the kinetic optical data surfaces was done using SPLMOD (*30*), as earlier described (*31*). The data from transmittance and

Table 1: Catalytic Activity and Proton Translocation by *P. denitrificans* Cytochrome *c* Oxidase Wild Type and Mutants

oxidase	O_2 consumption activity (% of wt)[a]	proton translocation (H^+/e^-) measured with spheroplasts[b]	proton translocation (H^+/e^-) measured with reconstituted enzyme[c]
wild type	100	2.8−3.1	0.7−0.9
W164F	40	2.5−2.7	0.4−0.5
D124N/W164F	5	ND	ND

[a] Activity is expressed as percent of WT activity (1000−1200 e^-/s/aa_3). For experimental conditions, see Materials and Methods. [b] Proton translocation in intact cells determined by succinate oxidation using the O_2-pulse method. A proton-to-electron ratio of 3 indicates proton translocation by cytochrome *c* oxidase, while a ratio closer to 2 means decreased proton translocation by cytochrome *c* oxidase; alternatively, if the turnover rate by the oxidase is very low, O_2 will be consumed by the quinol oxidase also present in the membrane, yielding a ratio of 2. In such conditions, the proton-pumping efficiency of the oxidase cannot be determined. [c] Proton translocation measured in reconstituted proteoliposomes using the O_2-pulse method with ascorbate as substrate. The proton-to-electron value for reconstituted enzyme has been corrected for the 0.5 H^+/e^- released from ascorbate upon oxidation. The measurements were performed at pH 7.0−7.4. (ND, not determined).

ATR-FTIR spectroscopy were analyzed and presented with IGOR pro (WaveMetrics Inc).

RESULTS

The W164F mutation decreases the turnover rate to about 40% of WT enzyme and lowers the proton pumping stoichiometry to ~0.5 H^+/e^- (Table 1, see also refs *9* and *32*). In contrast to previous reports (*9*), no severe structural changes were detected in the mutant by optical or FTIR spectroscopy. Figure 2A shows the low-temperature light-minus-dark FTIR CO difference spectra of W164F and WT enzymes. For the aa_3-type heme-copper oxidase the Fe_{a3}−CO stretching frequency can assume two different conformations (*33*), the α conformation with a characteristic trough around 1966 cm^{-1} and the β conformation with a trough around 1953 cm^{-1}. The coupled Cu_B−CO vibrations are mainly characterized by a positive peak around 2066 cm^{-1}. As seen in Figure 2A, no large shifts in the frequencies of either the Fe_{a3}−CO or the Cu_B−CO vibrations are observed when W164F is compared to WT enzyme. However, the 1966 cm^{-1} band of the α conformation of Fe_{a3}−CO appears to be split into two close-lying bands, which indicates that the structure of the binuclear center is somewhat perturbed in the mutant enzyme.

The effect of the W164F mutation on the heme *a*/heme a_3 surroundings was studied using ATR-FTIR spectroscopy. The reduced-minus-oxidized difference spectra of W164F and WT enzyme in the 1800−1350 cm^{-1} region at pH 6.5 are shown in Figure 2B. The trough at 1747−1745 cm^{-1} and the peak at 1738−1736 cm^{-1} have been ascribed to the protonated E278 in the *P. denitrificans* enzyme (*34*). In the mutant, both the peak and the trough decrease in amplitude relative to WT and may shift as well. The position of the C═O vibration of glutamic acid critically depends on hydrogen bonding and the environment, which is clearly changed in the mutant. Another difference in the spectrum of the mutant enzyme is a 4 cm^{-1} shift of the trough at ~1674 cm^{-1}. This area contains C═O vibrations from protonated propionates (*8*). A similar shift appears in WT

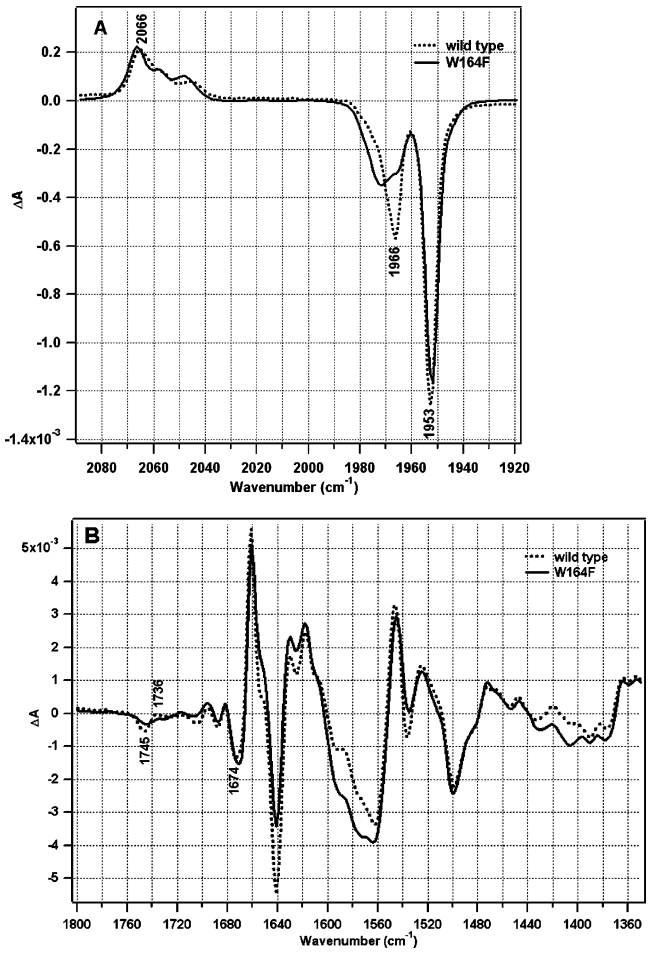

FIGURE 2: (A) Low-temperature light-minus-dark FTIR CO difference spectra of fully reduced, CO inhibited WT (dotted line) and W164F (solid line) enzyme at pD 6.5. The WT and the W164F spectrum are an average of 3520 scans performed at 210 respective 230 K with 2 cm^{-1} resolution. Normalization was done using the integrated intensities of the Fe_{a3}−CO peaks. The characteristic Fe_{a3}−CO troughs at 1953 and 1966 cm^{-1} and Cu_B-CO peak at 2066 cm^{-1} have been marked in the WT spectrum. (B) The reduced-minus-oxidized ATR FTIR difference spectra of WT (dotted line) and the W164F mutant (solid line) at pH 6.5. The carboxylic acid vibrations of E278 in reduced (~1736 cm^{-1}) respective oxidized (~1745 cm^{-1}) enzyme are shown. The negative trough at ~1674 cm^{-1} may be attributed to C═O vibrations of protonated propionates. The traces have been normalized to the optical absorption spectra of the reduced enzyme. The WT and W164F traces are the average of 12800 and 19200 interferograms, respectively. The resolution is 4 cm^{-1}. For other experimental conditions see Materials and Methods.

enzyme when the pH is changed from 6.5 to 9.0 (data not shown, see ref *35*), but in the mutant the trough remained at 1670 cm^{-1} at both pH values. Behr et al. (*9*) observed such a shift in the R473K and H403A mutants of the *Paracoccus* enzyme and ascribed it to loss of an arginine vibration and to the protonated ring A propionate of heme a_3, respectively. The former assignment seems unlikely because this vibration is insensitive to ^{15}N-isotope labeling (*35*). The loss of the pH-dependence of this feature in the mutant indicates that the mutation mimics high pH conditions in the propionate domain (Figure 1). Additional vibrational shifts appeared for the W164F mutant in the area around 1570 and 1400 cm^{-1}, which have been attributed to antisymmetric and symmetric stretches of deprotonated propionate carboxyls, respectively (*8*). However, these data do not allow any far-reaching

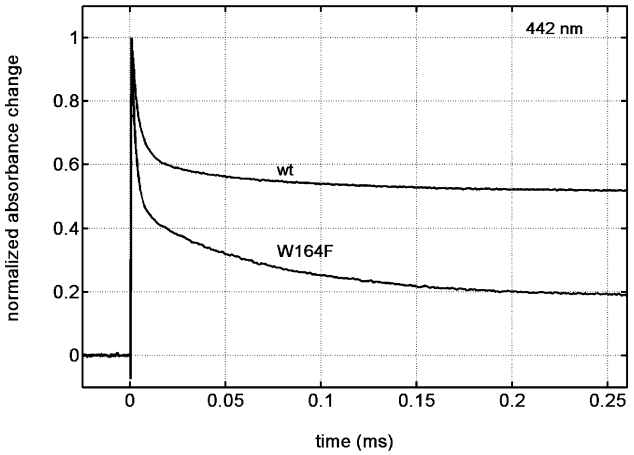

FIGURE 3: The normalized absorbance changes at 442 nm for W164F and WT after CO photolysis from COMV enzyme. Mixed-valence enzyme was formed by incubation of the oxidized enzyme with 1 atm CO. Experimental conditions: 100 mM HEPES−KOH, pH 8.0, 0.02% DM and 7 μM enzyme.

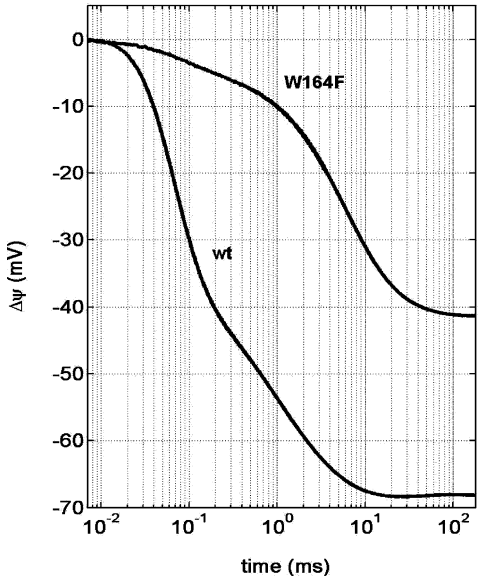

FIGURE 4: The electric potential generated for W164F and WT at pH 8.0 after oxygen addition to fully reduced enzyme. In WT, the amplitude is equally divided between the fast and slower transitions and has a maximum amplitude of 65−70 mV. For the W164F mutant, the total amplitude generated is ~40 mV of which only ~12% is generated in the fast phase. For experimental conditions see Materials and Methods.

conclusions with respect to perturbations of the propionate groups, which would require further labeling studies.

The rates and amplitudes of electron transfer between the different redox centers of cytochrome *c* oxidase depend on their respective midpoint redox potentials and can be measured optically by the "backflow method" (see Materials and Methods). The normalized absorption change at 442 nm of WT and W164F enzyme following CO photolysis from COMV enzyme is shown in Figure 3. The amplitude of the heme $a_3 \rightarrow$ heme *a* electron transfer is almost twice larger in W164F than in WT, but the rate is not affected significantly ($\tau \sim 3$ μs). The increase in amplitude in the mutant enzyme is due to a decrease in the midpoint redox potential (E_m) of heme a_3 relative to that of heme *a* but does not distinguish whether the E_m of heme a_3 decreases or the E_m of heme *a* increases or both. The amplitude of the second phase in the electron backflow reaction is due to slower electron equilibration between the heme groups and Cu_A ($\tau \sim 50$ μs) and reaches a maximum in the three electron reduced enzyme (*22*). In the mutant enzyme, Cu_A is reduced to almost 30% in this phase, compared to less than about 12% in WT. Since it is unlikely that the mutation has raised the redox potential of Cu_A, this latter result means that the E_m of one or both hemes has been lowered. Combining the results on electron backflow, we may therefore conclude that the mutation causes a decrease of the midpoint redox potential of heme a_3. The rate of CO recombination to mixed-valence enzyme verified the increased degree of electron backflow in the mutant. The CO recombination rate, which is proportional to the extent of reduction of heme a_3, was about four times slower for W164F compared to WT. This corresponds to a ~50 mV decrease in the E_m of heme a_3, which was confirmed by spectroelectrochemical redox titrations (data not shown). The increase in driving force for electron transfer may be expected to also increase the rate. However, for a true electron-tunneling event the expected effect is at most a factor of 2 and thus difficult to discern. Moreover, the 3 μs rate of electron backflow is likely to be limited by CO-dissociation from Cu_B (*36*, *37*).

A combination of the classical flow-flash method of Gibson and Greenwood (*24*) with time-resolved electrometry (*21*) was used to study the rates and amplitudes of membrane potential generation during oxidation of the fully reduced enzyme by O_2. Here, the fully reduced enzyme first reacts with O_2 to form the dioxygen adduct, compound **A**, which decays to the $\mathbf{P_R}$ state with transfer of the electron from heme *a* to the binuclear center and scission of the O−O bond (*38*). This early part of the reaction has not previously been found to be associated with formation of membrane potential but has been attributed to occur during a lag in the electrometric trace [(*22*), Figure 4, but see below]. Then follows the $\mathbf{P_R} \rightarrow \mathbf{F}$ and $\mathbf{F} \rightarrow \mathbf{O}$ reaction steps, which in WT enzyme are associated with about equal amplitudes of membrane potential formation. Figure 4 shows the electric potential generated when fully reduced WT and W164F enzymes are allowed to react with oxygen. After the lag, the membrane potential is generated in three phases. In WT enzyme the first phase has a time constant of ~50 μs, constitutes 50% of the whole amplitude generated, and corresponds kinetically to the optically detected $\mathbf{P_R} \rightarrow \mathbf{F}$ transition. It has been interpreted to result from pumping of one proton across the membrane and uptake of a substrate proton by the binuclear center. In the same phase, the fourth electron at Cu_A is equilibrated with heme *a*, which also contributes to the electrogenicity.

The time constant for this first phase of membrane potential generation is twice slower in the W164F mutant compared to WT, but more interestingly, it accounts for only ~12% of the total amplitude generated (Figure 4). In addition, the lag appears to be shorter in the mutant enzyme, mean values being 12 and 30 μs for mutant and WT, respectively. The amplitude roughly corresponds to translocation of one charge across 30% of the dielectric (see Materials and Methods) and is clearly too small to account for full proton translocation and even for uptake of a substrate proton from the aqueous N-side into the binuclear center (see Discussion). However, a competing back leak of protons from the P-side of the membrane to the binuclear center

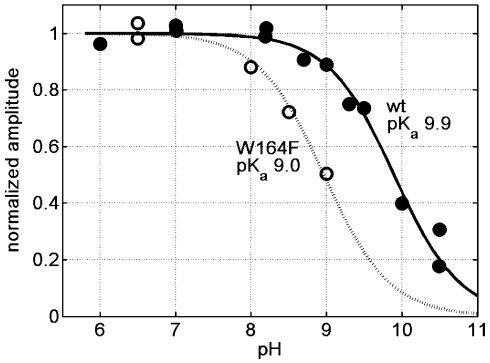

FIGURE 5: pH dependence of the development of membrane potential when fully reduced W164F and WT enzyme reacts with oxygen. The pH dependence was fitted with the Henderson−Hasselbalch equation and resulted in a pK_a ~9.0 for W164F and a pK_a ~9.9 for WT enzyme. The experimental conditions are described in Materials and Methods.

might decrease the net amplitude. This possibility was tested by combining the W164F mutation with the well-known D-pathway mutation D124N (*39*, *40*), which very effectively blocks proton transfer from the N-side, but the same small amplitude of the fast phase (~12% of total $\Delta\psi$ generated) was again observed (data not shown). A back leak of protons from the P-side in the single mutant W164F cannot therefore explain the low amplitude of the fast electrometric transition. In such a case, the double mutation would have resulted in a further decrease in the amplitude, or even a reverse in sign, due to the nearly complete blockage of proton transfer along the D-pathway by the additional D124N mutation (but, see below).

In WT enzyme, the fast phase of membrane potential generation is followed by two slower phases with time constants of ~200 μs and ~1.3 ms through which the enzyme is cycled back to the oxidized state **O** (Figure 4). Together, these slower phases constitute ca. 50% of the total amplitude generated and are explained as due to uptake of one additional substrate proton for water formation accompanied by pumping of one proton. The time constants for the electrometric **F** → **O** transition (0.2 and 1.3 ms in WT enzyme) are slowed significantly in the mutant (5−7 and 14−20 ms), but the amplitude remains essentially unchanged (Figure 4).

A clear difference between W164F and WT enzyme was also noted in the pH dependence of the total electric potential generated during the reaction of the fully reduced enzyme with oxygen (Figure 5). At high pH, the amplitude of membrane potential generation decreases drastically in WT enzyme. This cannot be attributed to an increased proton permeability of the liposomes because the spontaneous decay of membrane potential is not accelerated with increased pH, the effect is reversible upon lowering the pH, and the oxygen reduction chemistry still occurs over the entire tested pH range. Therefore, the effect of high pH must be attributed to a leak of protons from the P-side into the binuclear center, as concluded by Mills and Ferguson-Miller for the equivalent of the D124N mutant in the enzyme from *Rhodobacter sphaeroides* (*13*), which blocks proton uptake via the D-pathway. The pH dependence can be fitted to an apparent pK_a of ~9.9 for WT enzyme, which is significantly lowered in the mutant. This effect suggests that high pH renders the enzyme susceptible to proton leaks from the P-side and that this leak is controlled by one or more pH-sensitive groups, the apparent proton affinity of which is decreased in the mutant. This result does not contradict the absence of such a leak near neutral pH during the fast electrometric phase.

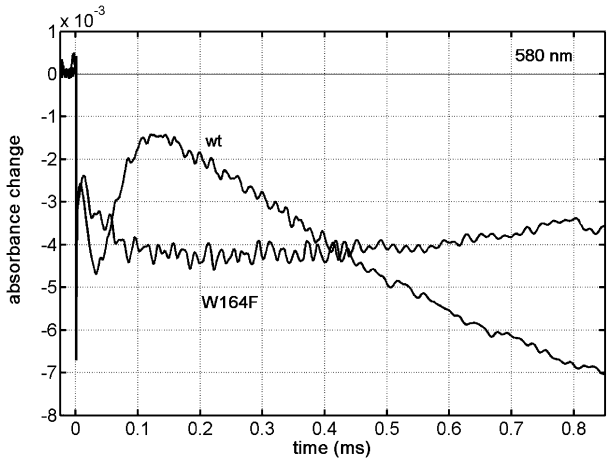

FIGURE 6: The flow-flash reaction of the fully reduced W164F and WT enzyme with oxygen recorded at 580 nm. The traces are normalized to the enzyme concentration. The laser was fired at time zero and this caused the photodissociation of CO, seen as a jump in absorption. Concentrations after mixing: 100 mM HEPES−KOH, pH 7.4, 0.02% DM, 3.4 mM potassium ascorbate, 0.8 μM TMPD, 5 μM enzyme, and 1 mM O_2.

The reaction between fully reduced W164F enzyme and oxygen was investigated at different single wavelengths using time-resolved optical flow-flash measurement (see Materials and Methods). Figure 6 shows the absorbance changes recorded at 580 nm where the appearance of the ferryl intermediate **F** has its maximum absorption (*41*). Also the primary dioxygen adduct, intermediate **A**, contributes to the absorption at this wavelength, although its absorption peak is at 595 nm (*42*). Formation of compound **A** was similar in W164F and WT, but a ca. 50% decrease in the rate of its decay into the $\mathbf{P_R}$ state is seen in the mutant (first downswing of the traces in Figure 6). However, **F** formation, seen as an increase in absorbance with a time constant of about 40 μs in WT enzyme, is slowed considerably in the mutant. At first sight, this result appears to disagree with the electrometric data, since in the W164F mutant the time constant of the fast electrometric phase, ascribed to the $\mathbf{P_R} \rightarrow \mathbf{F}$ transition in WT, was only twice slower. Optical flow-flash experiments on a slower time scale show that intermediate **F** eventually forms in the mutant enzyme, at a time of a few milliseconds, since further decay from this time domain to the **O** state is associated with the appearance of the characteristic absorption band of the **O** state at 660 nm, together with a trough at 580 nm showing decay of **F** (data not shown). The time constant of this change corresponds to the slowest phases in the electrometric measurement. We thus conclude that one clue for why the fast electrometric phase has such a low amplitude in the mutant enzyme is that it does not include formation of the **F** state, as it does in WT enzyme (see Discussion).

Absorbance changes at 445 or 605 nm give information about the oxidation of both Fe_a and Fe_{a3} during reduction of oxygen. At 445 nm (Figure 7), the initial oxygen binding ($\mathbf{R} \rightarrow \mathbf{A}$) and the oxidation of both heme a_3 and heme a during the $\mathbf{A} \rightarrow \mathbf{P_R}$ transition are difficult to separate from

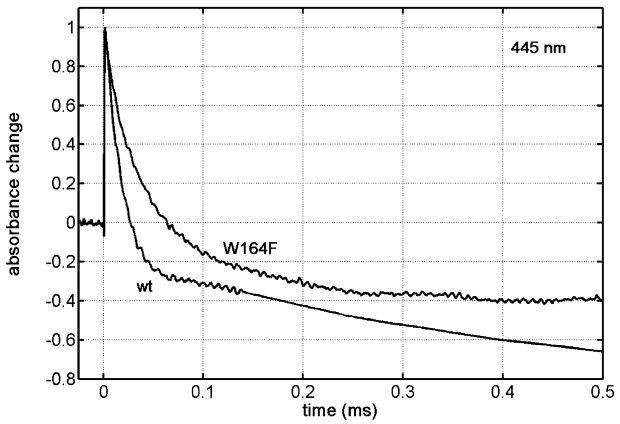

FIGURE 7: The flow-flash reaction of the fully reduced W164F and WT enzyme with oxygen recorded at 445 nm. The traces are normalized to the CO photolysis. The enzyme concentration after mixing was 2.5 μM. Other conditions are the same as in Figure 6. Laser flash at time zero.

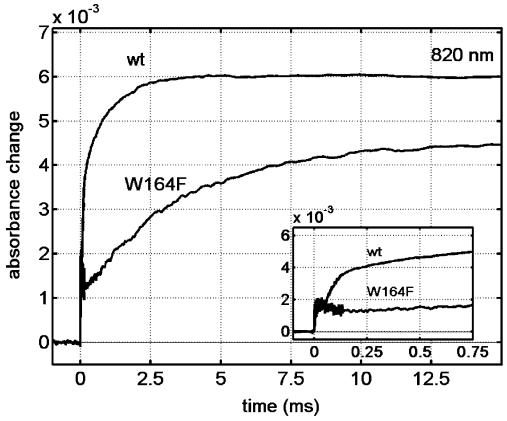

FIGURE 8: The reaction of the fully reduced W164F and WT enzyme with oxygen recorded at 820 nm. The traces are normalized to the total enzyme concentration. The inset shows the first 1 ms of the reaction. The enzyme concentration after mixing was ~8 μM. Other conditions after mixing were as described in Figure 6. The laser was fired at time zero.

one another and are normally detected as one phase with a time constant of ~30 μs in WT enzyme. Next, a plateau (~60 μs) appears, as heme *a* is re-reduced due to electron equilibration between Cu_A and heme *a*, which is associated with the $\mathbf{P_R} \rightarrow \mathbf{F}$ transition that in itself contributes very little to the absorption changes in the Soret region (*42*, *43*). The last phase seen is attributed to the final oxidation of the enzyme and has a time constant of ~1 ms in WT enzyme. In contrast, only two phases could be resolved at 445 nm for the W164F mutant. The first, with a time constant of ~40 μs, is most likely due to the $\mathbf{R} \rightarrow \mathbf{A}$ transition and the decay of **A**, since the recordings at 580 (Figure 6) and 595 nm (not shown) indicated no large changes in the time constants of formation and disappearance of compound **A**. The second phase, however, with a time constant of 200−500 μs is at least four times slower than the fast phase attributed to heme *a* re-reduction during the $\mathbf{P_R} \rightarrow \mathbf{F}$ transition in WT enzyme. Moreover, the ~500 μs phase in the mutant cannot represent heme *a* re-reduction which gives a change of opposite sign. These results suggest a change in the mutant with respect to the fast re-reduction of heme *a* by Cu_A. To test this, we studied oxidation of Cu_A at 820 nm directly (Figure 8). In WT enzyme, the initial fast rise and decline in absorbance is caused by the formation and decay of compound **A**, and this is similar in the mutant, confirming the data at other wavelengths (see above). This is followed by a large biphasic rise in absorbance with time constants of ~50 μs and ~1 ms. The 50 μs phase is due to Cu_A oxidation by heme *a* during the $\mathbf{P_R} \rightarrow \mathbf{F}$ transition, while the millisecond phase represents Cu_A oxidation during the $\mathbf{F} \rightarrow \mathbf{O}$ step. In the W164F mutant, much slower Cu_A oxidation was observed ($\tau \sim 3.5$ ms for the first phase, Figure 8). This shows that there is no fast partial re-reduction of heme *a* by Cu_A in the mutant, which explains the kinetics observed at 445 nm (Figure 7). It is known from work with mutants of the *R. sphaeroides* enzyme that the partial oxidation of Cu_A during the $\mathbf{P_R} \rightarrow \mathbf{F}$ transition is controlled by proton uptake through the D-pathway (*44*, *45*). The immediate proton donor to the binuclear center is the conserved residue E278, which is normally quickly reprotonated in a non-rate-limiting reaction. Hence, the much decelerated oxidation of Cu_A in the mutant is best explained by failure to quickly reprotonate E278 from the N-side via the D-pathway. Whilst such an effect is expected from a block in the D-pathway, it is a surprising consequence of the present mutation, which lies far above the E278 site (Figure 1; see Discussion).

Species equivalent to the $\mathbf{P_M}$ and **F** intermediates are produced when oxidized cytochrome *c* oxidase from *P. denitrificans* reacts with H_2O_2, as has previously been described for the enzymes from bovine heart (*46*), *R. sphaeroides* (*47*), and the *Escherichia coli* cytochrome bo_3 enzyme (*48*−*50*). Pecoraro et al. (*47*) showed that two species were produced sequentially, analogous to compounds I and II in peroxidases. At high pH, intermediate I has an optical spectrum very similar to state $\mathbf{P_M}$ of the binuclear center, whereas intermediate II has the properties of the **F** state (see also refs *46* and *51*−*53*). At low pH, intermediate I consists of a mixture of state $\mathbf{P_M}$ and an isoelectronic **F**-like state called **F′**. Vygodina et al. (*54*) reported with oxidase vesicles that this pH dependence is mediated from the N-side of the membrane, and Pecoraro et al. (*47*) found that the pH dependence was abolished by a mutation in the K-pathway, so that the peroxide reaction yielded $\mathbf{P_M}$ also at low pH. Both Pecoraro et al. (*47*) and Junemann et al. (*46*) proposed a branched scheme of the peroxide reaction to account for these data, implying that the $\mathbf{P_M}$ and **F′** states are not in rapid equilibrium (see also ref *55*). All work this far agrees with the notion that the most likely structure of **F′** is one where Cu_B[II] has an aquo ligand while this ligand is a hydroxide in $\mathbf{P_M}$.

Figure 9 shows the optical spectra of the first intermediate formed when newly oxidized WT and W164F enzymes were allowed to react with 10 mM H_2O_2 at different pH values. At high pH (9.5), the reaction between WT enzyme and H_2O_2 quickly yields compound $\mathbf{P_M}$, recognized by its typical absorption spectrum (Figure 9A). The optical spectrum of the second intermediate is compound **F**, which forms with decay of the $\mathbf{P_M}$ intermediate (spectra not shown). However, at low pH (6.5) the reaction between WT enzyme and H_2O_2 yields less of the $\mathbf{P_M}$ intermediate and, in the same kinetic phase, also an **F**-like species with an absorption maximum around 575 nm that has been called **F′** (or $\mathbf{F^{\bullet}}$, or "fast **F**") (*46*−*50*). In contrast to compound **F**, the **F′** state contains only two reducing equivalents in the binuclear center being

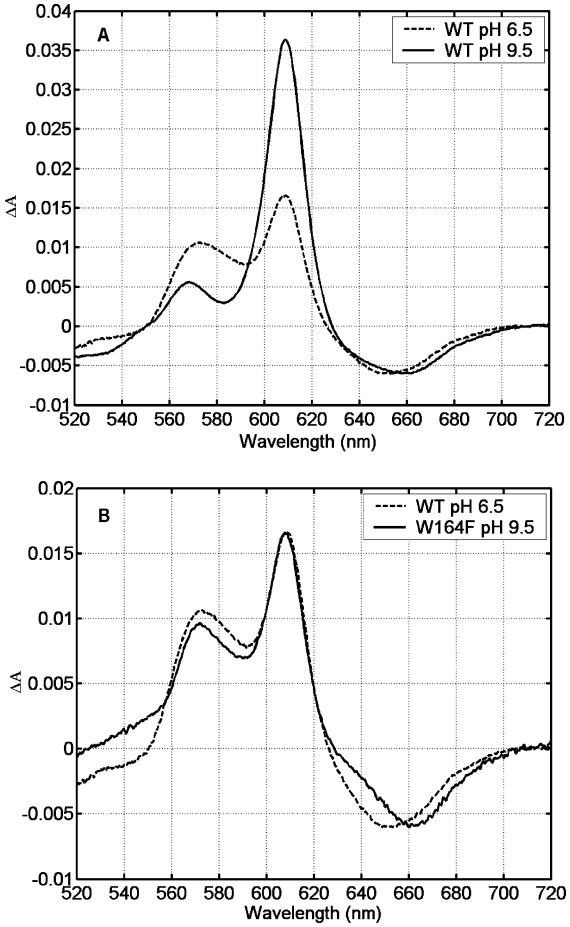

FIGURE 9: The optical spectra of the first intermediate formed when newly oxidized WT and W164F enzyme are allowed to react with H_2O_2. (A) WT pH 6.5 (dotted line) and pH 9.5 (solid line). (B) WT pH 6.5 (dotted line) and W164F pH 9.5 (solid line). Conditions after mixing: 100 mM buffer, 0.025% DM, 7 μM enzyme, and 10 mM H_2O_2. For detailed experimental conditions see Materials and Methods.

isoelectronic with $\mathbf{P_M}$. The relative extent of $\mathbf{P_M}$ and $\mathbf{F'}$ intermediates formed with H_2O_2 is pH-dependent with an apparent pK_a of 6.7−7.3 in the bovine enzyme (*46*, *54*). When the W164F mutant is allowed to react with H_2O_2 under the same conditions, a substantial amount of $\mathbf{F'}$ is formed also at high pH (Figure 9B). The data with WT enzyme indicated a pK_a of ~7 for this phenomenon in the *P. denitrificans* enzyme (not shown, see refs *46*, *54*, and *55*). In the W164F mutant, this apparent pK_a is raised about 2 pH units**,** favoring formation of $\mathbf{F'}$ over $\mathbf{P_M}$ also at a pH higher than neutrality. This indicates a pK_a shift of an acidic site close to the binuclear center by the mutation, the protonation state of which controls whether the product of the peroxide reaction is $\mathbf{P_M}$ or $\mathbf{F'}$. According to this scenario, the mutation would favor the pathway that is linked to proton uptake via the K-pathway, which forms $\mathbf{F'}$ exclusively (*47*).

DISCUSSION

The simplest explanation for the pH effect on the product formed in the reaction of oxidized enzyme with H_2O_2 is that the initial **O** state can take up a proton to a group with pK_a ~7, and that the product of the subsequent peroxide reaction depends on whether this proton is bound initially or not. However, Pecoraro et al. (*47*) found that preincubation of

Scheme 1

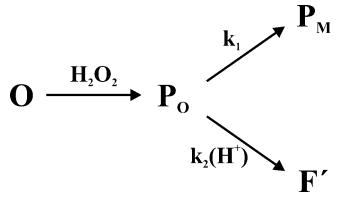

Scheme 2

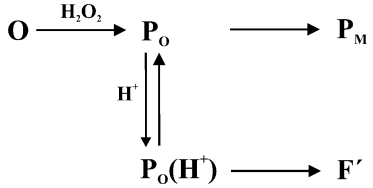

the K-pathway mutant enzyme at low pH did not diminish formation of $\mathbf{P_M}$; neither did it yield formation of $\mathbf{F'}$, both of which would have been expected if the protonation occurs already before the reaction with peroxide. They consequently proposed a reaction scheme (Scheme 1) with two kinetically competing pathways leading from a common "peroxy intermediate" ($\mathbf{P_o}$) to either $\mathbf{P_M}$ or $\mathbf{F'}$, where the latter route is governed by a pH-dependent rate constant.

This is a purely kinetic model where it is assumed that the observed pK_a is only apparent and a function of the relative rates of the two competing reactions, one of which is pH-dependent. Although the rate of formation of these intermediates was not appreciably pH-dependent, this may be explained if the initial bimolecular formation of $\mathbf{P_o}$ is rate-limiting (Scheme 1). This rate is about 500 M^{-1} s^{-1} (*46*, *47*), which yields 50 s^{-1} at the highest tested H_2O_2 concentration (100 mM) where the observed rate is still linearly dependent on [H_2O_2]. The rates of the reaction branches from $\mathbf{P_o}$ to $\mathbf{P_M}$ and to $\mathbf{F'}$ must therefore be faster than this. Cautiously assuming 100 s^{-1} for the rate for the former reaction (k_1), the proton-dependent rate constant of the second branch must be 10^9 M^{-1} s^{-1} to yield the apparent pK_a of 7 for the relative amplitudes of $\mathbf{P_M}$ and $\mathbf{F'}$ formation; a higher rate for k_1 would require an even faster rate of k_2, but 10^9 M^{-1} s^{-1} already seems very fast for proton transfer via the K-pathway. On the other hand, a rate of only 100 s^{-1} for k_1 stands in contrast to the known rate of >5000 s^{-1} for splitting the O−O bond in the reaction of cytochrome oxidase with O_2 (*56*). Moreover, following this reaction model, the effect of the W164F mutation must be a relative block of k_1 (Scheme 1). The two-unit rise in the apparent pK_a then means that the rate constant k_1 must be decreased by 2 orders of magnitude by the mutation. This may be tested in future work because it predicts that formation of $\mathbf{P_o}$ is no longer rate-limiting in the mutant enzyme.

However, we may also consider an alternative reaction scheme where the observed pK_a is real, viz. the pK_a of the heme a_3-bound peroxide (in state $\mathbf{P_o}$, Scheme 2). It may be envisaged, for example, that hydrogen peroxide binds to the binuclear center having two OH^- ligands (one on Cu_B and one on heme iron), forming a transient $\mathbf{P_o}$ state with a deprotonated peroxide bridge between the metals and two water molecules. If the pK_a of bound hydroperoxide is ~7 and the pH is near neutral or lower, the peroxide may be protonated via the K-pathway. The result is a transient pH-

dependent mixture of peroxide and hydroperoxide bound to heme a_3, of which the former forms $\mathbf{P_M}$ (OH-bound to Cu_B) and the latter $\mathbf{F'}$ (H_2O bound to Cu_B) upon heterologous splitting of the peroxide O−O bond. As proposed by Pecoraro et al. (*47*), the formation of the ferryl heme a_3 species in both branches of the reaction blocks the K-pathway so that fast protonic equilibration is no longer possible between the two end products. In this scenario, the controlling protonatable site is the bound peroxide itself. The W164F mutation abolishes the strong hydrogen bond from W164 to the heme a_3 Δ-propionate, which was found to cause a considerable downshift of the E_m of this heme (see Results). Therefore, it is conceivable that the mutation may cause a two-unit upshift in the pK_a of the Fe[III]-OOH structure of heme a_3, favoring the hydroperoxide ligand and formation of the $\mathbf{F'}$ state at pH values well above 7.

The most striking effect of the W164F mutation is the dramatically lowered amplitude of the first phase of membrane potential development when the enzyme reacts with O_2. The amplitude of this phase, which has been ascribed to the $\mathbf{P_R} \rightarrow \mathbf{F}$ transition in WT enzyme, is far too small in the mutant to be ascribed to uptake of a substrate proton into the heme a_3/Cu_B center from the aqueous N-side (1 charge equivalent across ca. 70% of the dielectric). It can also not be due to electron transfer from Cu_A to heme *a*, because this process was found to be decelerated into the millisecond regime. We further excluded that the small amplitude might be due to partial proton leakage into the membrane from the P-side (see Results). The delay of **F** formation in the mutant provides at least part of the explanation for the low amplitude, because formation of **F** includes electrogenic uptake of a proton from the N-side into the binuclear center. Clearly, in the mutant the fast electrometric phase occurs prior to the $\mathbf{P_R} \rightarrow \mathbf{F}$ transition and its kinetics actually match the preceding $\mathbf{A} \rightarrow \mathbf{P_R}$ step (see below).

Deceleration of both Cu_A oxidation and **F** formation suggests that the mutation slows down proton uptake to E278 via the D-pathway. Such an effect is surprising considering the position of W164 in the structure relative to the D-pathway (Figure 1) but may be rationalized by considering the properties of E278. For E278 to catalyze proton transfer from the D-pathway for pumping, or for proton transfer to the binuclear center, the E278 side chain has been proposed to rotate from the downward position in the X-ray structure, where it connects to the D-pathway, to an upward position closer to the P-side of the membrane, and back (*57*−*59*). Replacement of W164 with the smaller phenylalanine will create space specifically near the putative "upward" position of the E278 side chain and lead to new packing, which may be explored by molecular dynamics simulations. Our simulations have shown that in the mutant the benzoid ring of phenylalanine assumes the position of the pyrrol ring of the tryptophan in the X-ray structure of WT enzyme. This indeed creates new space for the E278 side chain in its "upward" position; in the WT structure this space is occupied by the benzoid ring of the tryptophan. Therefore, the W164F mutation may favor a position of the E278 side chain where it is not in contact with the D-pathway, which would explain why reprotonation of E278 via the D-pathway is decelerated. Changes of the FTIR spectrum were indeed detected in the mutant enzyme indicating a change in the surroundings of the carboxyl group of E278 (Figure 2B). Our data thus provide further support for the notion that the E278 side chain must undergo conformational isomerization from its X-ray position to achieve its proton-transferring function because the space created by the mutation is far above the crystallographic position of the E278 side chain, and yet the basic phenotype of the mutation implies a block of protonation of this residue via the D-pathway.

The amplitude of the slow electrometric phase is about the same in the mutant as in WT enzyme. We believe that this is purely fortuitious and due to retardation of electrogenic events that normally occur during the fast phase. Formation of the **F** state in the mutant is strongly delayed and merges, in part, with the subsequent $\mathbf{F} \rightarrow \mathbf{O}$ transition. This means that the second electrometric phase will include uptake of *two* substrate protons into the binuclear center, due to formation of **F** and during $\mathbf{F} \rightarrow \mathbf{O}$. The slow phase will moreover include the electrogenic transfer of the electron from Cu_A to the binuclear center (via heme *a*), and any proton transfers due to proton pumping (see below). This "reshuffling" of electrogenic events from the first to the second electrogenic transition in the mutant (compared to WT) readily accounts for the observation that the amplitude of the slow phase in the mutant is of a similar magnitude as in WT.

The lack of proton transfer to the binuclear center during the fast electrometric phase in the mutant enzyme thus helps to explain its low amplitude. More significantly, the early onset of this phase in the mutant (with a time constant similar to $\mathbf{A} \rightarrow \mathbf{P_R}$) suggests that such an early small-amplitude electrometric phase may also take place in the WT enzyme, where it could easily be missed due to the high amplitude charge translocation during the immediately following $\mathbf{P_R} \rightarrow \mathbf{F}$ transition. In fact, this early electrogenic phase is not unique to the W164F mutant enzyme but may also be observed in other conditions where the strong electrogenicity of the $\mathbf{P_R} \rightarrow \mathbf{F}$ transition is suppressed (Belevich et al., in preparation). What, then, could be the nature of this fast charge transfer reaction? It is most likely due to proton transfer because electron transfer from heme *a* to the binuclear center during $\mathbf{A} \rightarrow \mathbf{P_R}$ occurs within the plane of the membrane. Although a small deviation from this arrangement of electron donor and acceptor relative to the membrane dielectric may be picked up by the current sensitive time-resolved technique, such electron transfer would hardly account for the observed amplitude, which is of the same order of magnitude as for electron transfer from Cu_A to heme *a*. Yet, this fast electrogenic proton transfer reaction is definitely coupled to the electron transfer from heme *a* to the binuclear center (with formation of the $\mathbf{P_R}$ state) because the data reported by Jasaitis et al. (*22*) excludes vectorial proton-transfer coupled to oxidation of the two-electron reduced (mixed valence) enzyme by O_2 to form the $\mathbf{P_M}$ state.

The only plausible proton donor for this reaction is E278 at the end of the D-pathway, but since **F** is not formed in this early time domain, the proton acceptor cannot be the binuclear center. Also, the amplitude is too high to be consistent with proton transfer from E278 to the binuclear center, since the distance between these sites is very short when projected on the membrane normal (Figure 1). From a functional point of view, it seems plausible that this event is an elementary step of the proton-pumping reaction: a

proton transfer from E278 to a "pump site" above the heme groups that fortuitously becomes visible in the W164F mutant due to the delay in the formation of the **F** intermediate. If this interpretation is correct, it has strong impact on the proton pump mechanism for several reasons. First, it suggests that electron transfer from heme *a* to the binuclear center is associated with transfer of a proton from E278 to a pump site, and that this precedes uptake of a proton to the binuclear center. Second, it suggests that the pump site is unoccupied in the **R** and **A** states. Finally, it is compatible with previous reports (*29*) that show full proton-pumping during the transition from state **R** to state **F**. Although all partial steps of proton-pumping were previously thought to occur during the $\mathbf{P_R} \rightarrow \mathbf{F}$ reaction in WT enzyme, this may now have to be revised such that the preceding $\mathbf{A} \rightarrow \mathbf{P_R}$ step is already associated with loading of the pump site from E278, which is followed, during $\mathbf{P_R} \rightarrow \mathbf{F}$, by reprotonation of E278 from the D-pathway, proton transfer from E278 to the binuclear center, a second protonation of E278 from the N-side and release of the proton from the pump site toward the N-side of the membrane.

Olsson et al. (*60*) recently concluded from a pioneering computational approach that proton transfer (via water molecules) from E278, either to the pump site or to the binuclear center, would encounter a far too high energetic barrier to yield reasonable kinetics, unless this process included concerted reprotonation of E278 via the D-pathway. This notion seems to be contradicted by the observation that formation of the **F** state in the canonical D-pathway mutant D124N is as fast as in WT enzyme both in cytochromes bo_3 from *E. coli* (*61*) and aa_3 from *R. sphaeroides* (*62*). However, there is no experimental evidence to date ensuring that E278 would not be reprotonated on a fast time scale in the D124N mutant, even though proton uptake from the N-side into the D-pathway is certainly blocked (*62*). Such reprotonation of E278 would obviously require a proton donor within the D-pathway above the D124 site. On the other hand, in the W164F mutant studied here, such reprotonation of E278 would have been readily detected as a large-amplitude charge transfer in the electrometric measurements. The high barrier against proton transfer from E278 (*60*) might, in part, be due to neglect of the side chain isomerization of this residue. In this connection, we note that the phenotype of the W164F mutation shows an interesting difference relative to the D124N mutant enzyme because only in the former is the rate of formation of the **F** state strongly delayed. This difference may be related to the expected difference in the rate-limiting step of proton transfer via E278. In the W164F mutant, the ionized E278 side chain is expected to be stalled in the "upward" position where there is no contact to the D-pathway. By contrast, in the D124N mutant the ionized E278 is free to move to the "downward" position where it makes contact with the D-pathway. Exploration of this difference in future experiments may yield further valuable insight into the proton-pumping mechanism.

ACKNOWLEDGMENT

We thank Eija Haasanen, Anne Hakonen, and Tarja Salojärvi for excellent technical assistance.

REFERENCES

1. Wikström, M. (2004) Cytochrome *c* oxidase: 25 years of the elusive proton pump, *Biochim. Biophys. Acta 1655*, 241−247.
2. Brzezinski, P. (2004) Redox-driven membrane-bound proton pumps, *Trends Biochem. Sci. 29*, 380−387.
3. Mills, D. A., and Ferguson-Miller, S. (2003) Understanding the mechanism of proton movement linked to oxygen reduction in cytochrome *c* oxidase: lessons from other proteins, *FEBS Lett. 545*, 47−51.
4. Wikström, M. (1977) Proton pump coupled to cytochrome *c* oxidase in mitochondria, *Nature 266*, 271−273.
5. Ädelroth, P., Gennis, R. B., and Brzezinski, P. (1998) Role of the Pathway through K(I-362) in Proton transfer in cytochrome *c* oxidase from *R. sphaeroides*, *Biochemistry 37*, 2470−2476.
6. Kannt, A., Lancaster, C. R. D., and Michel, H. (1998) The coupling of electron transfer and proton translocation: electrostatic calculations on *Paracocus denitrificans* cytochrome *c* oxidase, *Biophys. J. 74*, 708−721.
7. Puustinen, A. and Wikström, M. (1999) Proton exit from the heme-copper oxidase of *Escherichia coli*, *Proc. Natl. Acad. Sci. U.S.A. 96*, 35−37.
8. Behr, J., Hellwig, P., Mäntele, W., and Michel, H. (1998) Redox dependent changes at the heme propionates in cytochrome *c* oxidase from *Paracoccus denitrificans*: Direct evidence from FTIR difference spectroscopy in combination with heme propionate ^{13}C labeling, *Biochemistry 37*, 7400−7406.
9. Behr, J., Michel, H., Mäntele, W., and Hellwig, P. (2000) Functional properties of the heme propionates in cytochrome *c* oxidase from *Paracoccus denitrificans*. Evidence from FTIR difference spectroscopy and site-directed mutagenesis, *Biochemistry 39*, 1356−1363.
10. Iwata, S., Ostermeier, C., Ludwig, B., and Michel, H. (1995) Structure at 2.8 Å resolution of cytochrome *c* oxidase from *Paracoccus denitrificans*, *Nature 376*, 660−669.
11. Tsukihara, T., Aoyama, H., Yamashita, E., Takashi, T., Yamaguichi, H., Shinzawa-Itoh, K., Nakashima, R., Yaono, R., and Yoshikawa, S. (1996) The whole structure of the 13-subunit oxidized cytochrome *c* oxidase at 2.8 Å, *Science 272*, 1136−1144.
12. Kawasaki, M., Mogi, T., and Anraku, Y. (1997) Substitutions of charged amino acid residues conserved in subunit I perturb the redox metal centers of the *Escherichia coli bo*-type ubiquinol oxidase, *J. Biochem. 122*, 422−429.
13. Mills, D. A. and Ferguson-Miller, S. (2002) Influence of structure, pH and membrane potential on proton movement in cytochrome oxidase, *Biochim. Biophys. Acta 1555*, 96−100.
14. Qian, J., Mills, D. A., Geren, L., Wang, K. F., Hoganson, C. W., Schmidt, B., Hiser, C., Babcock, G. T., Durham, B., Millett, F., and Ferguson-Miller, S. (2004) Role of the conserved arginine pair in proton and electron transfer in cytochrome *c* oxidase, *Biochemistry 43*, 5748−5756.
15. Brändén, G., Brändén, M., Schmidt, B., Mills, D. A., Ferguson-Miller, S., and Brzezinski, P. (2005) The protonation state of a heme propionate controls electron transfer in cytochrome *c* oxidase, *Biochemistry 44*, 10466−10474.
16. Mills, D. A., Geren, L., Hiser, C., Schmidt, B., Durham, B., Millett, F., and Ferguson-Miller, S. (2005) An arginine to lysine mutation in the vicinity of the heme propionates affects the redox potentials of the hemes and associated electron and proton transfer in cytochrome *c* oxidase, *Biochemistry 44*, 10457−10465.
17. Riistama, S., Laakkonen, L., Wikström, M., Verkhovsky, M. I., and Puustinen, A. (1999) The Calcium Binding Site in Cytochrome aa_3 from *Paracoccus denitrificans*, *Biochemistry 38*, 10670−10677.
18. Puustinen, A., Finel, M., Virkki, M., and Wikström, M. (1989) Cytochrome *o*(*bo*) is a Proton Pump in *Paracoccus denitrificans* and *Escherichia coli*, *FEBS Lett. 249*, 163−167.
19. Rigaud, J. L., Pitard, B., and Levy, D. (1995) Reconstitution of membrane proteins into liposomes: application to energy-transducing membrane proteins, *Biochim. Biophys. Acta 1231*, 223−246.
20. Backgren, C., Hummer, G., Wikström, M., and Puustinen, A. (2000) Proton translocation by cytochrome *c* oxidase can take place without the conserved glutamic acid in subunit I, *Biochemistry 39*, 7863−7867.
21. Drachev, L. A., Jasaitis, A. A., Kaulen, A. D., Kondrashin, A. A., Liberman, E. A., Nemecek, I. B., Ostroumov, S. A., Semenov, A. Y., and Skulachev, V. P. (1974) Direct measurement of electric current generation by cytochrome oxidase, H^+-ATPase and bacteriorodopsin, *Nature 249*, 321−324.
22. Jasaitis, A., Verkhovsky, M. I., Morgan, J. E., Verkhovskaya, M. L., and Wikström, M. (1999) Assignment and charge translocation

stoichiometries of the major electrogenic phases in the reaction of cytochrome *c* oxidase with dioxygen, *Biochemistry 38*, 2697−2706.
23. Verkhovsky, M. I., Morgan, J. E., and Wikström, M. (1992) Intramolecular electron transfer in cytochrome *c* oxidase: a cascade of equilibria, *Biochemistry 31*, 11860−11863.
24. Gibson, Q. H. and Greenwood, C. (1963) Reactions of cytochrome oxidase with oxygen and carbon monoxide, *Biochem. J. 86*, 541−554.
25. Riistama, S., Puustinen, A., Verkhovsky, M. I., Morgan, J. E., and Wikström, M. (2000) Binding of O_2 and its reduction are both retarded by replacement of valine 279 by isoleucine in cytochrome *c* oxidase from *Paracoccus denitrificans*, *Biochemistry 39*, 6365−6372.
26. Iwaki, M., Puustinen, A., Wikström, M., and Rich, P. R. (2003) ATR-FTIR spectroscopy of the P_M and F intermediates of bovine and *Paracoccus denitrificans* cytochrome *c* oxidase, *Biochemistry 42*, 8809−8817.
27. Rich, P. R., and Breton, J. (2002) Attenuated total reflection Fourier transform infrared studies of redox changes in bovine cytochrome *c* oxidase: resolution of the redox Fourier transform infrared difference spectrum of heme a_3, *Biochemistry 41*, 967−973.
28. Bloch, D., Belevich, I., Jasaitis, A., Ribacka, C., Puustinen, A., Verkhovsky, M. I., and Wikström, M. (2004) The catalytic cycle of cytochrome *c* oxidase is not the sum of its two halves, *Proc. Natl. Acad. Sci. U.S.A. 101*, 529−533.
29. Verkhovsky, M. I., Jasaitis, A., Verkhovskaya, M. L., Morgan, L., and Wikström, M. (1999) Proton translocation by cytochrome *c* oxidase, *Nature 400*, 480−483.
30. Provencher, S. W., and Vogel, R. H. (1983) Regularization Techniques for Inverse Problems in Molecular Biology, in *Progress in Scientific Computing* (Deuflhard, P. and Hairer, E., Eds.) pp 304−319, Birkhauser, Boston.
31. Morgan, J. E., Verkhovsky, M. I., Puustinen, A., and Wikström, M. (1995) Identification of a "peroxy" intermediate in cytochrome bo_3 of *Escherichia coli*, *Biochemistry 34*, 15633−15637.
32. Wikström, M., Ribacka, C., Molin, M., Laakkonen, L., Verkhovsky, M., and Puustinen, A. (2005) Gating of proton and water transfer in the respiratory enzyme cytochrome *c* oxidase, *Proc. Natl. Acad. Sci. U.S.A. 102*, 10478−10481.
33. Alben, J. O. (1996) Fourier transform infrared spectroscopy of enzyme systems, in *Infrared Spectroscopy of Biomolecules* (Mantsch, H. H., Chapman, D., Eds.) pp 19−37, John Wiley & Sons, Inc., Publications, New York.
34. Hellwig, P. (1996) Carboxyl group protonation upon reduction of the *Paracoccus denitrificans* cytochrome *c* oxidase: direct evidence by FTIR spectroscopy, *FEBS 385*, 53−57.
35. Iwaki, M., Puustinen, A., Wikström, M., and Rich, P. R. (2004) ATR-FTIR spectroscopy and isotope labeling of the P_M intermediate of *Paracoccus denitrificans* cytochrome *c* oxidase, *Biochemistry 43*, 14370−14378.
36. Verkhovsky, M. I., Jasaitis, A., and Wikström, M. (2001) Ultrafast haem-haem electron transfer in cytochrome *c* oxidase, *Biochim. Biophys. Acta 1506*, 143−146.
37. Pilet, E., Jasaitis, A., Liebl, U., and Vos, M. H. (2004) Electron transfer between hemes in mammalian cytochrome *c* oxidase, *Proc. Natl. Acad. Sci. U.S.A 101*, 16198−16203.
38. Morgan, J. E., Verkhovsky, M. I., Palmer, G., and Wikström, M. (2001) Role of the P_R Intermediate in the Reaction of Cytochrome *c* Oxidase with O_2, *Biochemistry 40*, 6882−6892.
39. Thomas, J. W., Puustinen, A., Alben, J. O., Gennis, R. B., and Wikström, M. (1993) Site-directed mutagenesis of highly conserved residues in helix VIII of subunit I of the cytochrome *bo* ubiquinol oxidase from *Escherichia coli*: An amphipathic transmembrane helix that may be important in conveying protons to the binuclear center, *Biochemistry 32*, 10923−10928.
40. Fetter, J. R., Qian, J., Shapleigh, J., Thomas, J. W., Garcia-Horsman, A., Schmidt, E., Hosler, J., Babcock, G. T., Gennis, R. B., and Ferguson-Miller, S. (1995) Possible proton relay pathways in cytochrome *c* oxidase, *Proc. Natl. Acad. Sci. U.S.A. 92*, 1604−1608.
41. Wikström, M. (1981) Energy-dependent reversal of the cytochrome oxidase reaction, *Proc. Natl. Acad. Sci. U.S.A. 78*, 4051−4054.
42. Hill, B. C. and Greenwood, C. (1984) The reaction of fully reduced cytochrome *c* oxidase with oxygen studied by flow-flash spectrophotometry at room temperature, *Biochem. J. 218*, 913−921.
43. Morgan, J. E., Verkhovsky, M. I., and Wikström, M. (1996) Observation and assignment of peroxy and ferryl intermediates in the reduction of dioxygen to water by cytochrome *c* oxidase, *Biochemistry 35*, 12235−12240.
44. Karpefors, M., Ädelroth, P., Zhen, Y. J., Ferguson-Miller, S., and Brzezinski, P. (1998) Proton uptake controls electron transfer in cytochrome *c* oxidase, *Proc. Natl. Acad. Sci. U.S.A. 95*, 13606−13611.
45. Ädelroth, P., Svensson, E. M., Mitchell, D. M., Gennis, R. B., and Brzezinski, P. (1997) Glutamate 286 in cytochrome aa_3 from *Rhodobacter sphaeroides* is involved in proton uptake during the reaction of the fully reduced enzyme with dioxygen, *Biochemistry 36*, 13824−13829.
46. Junemann, S., Heathcote, P., and Rich, P. R. (2000) The reactions of hydrogen peroxide with bovine cytochrome *c* oxidase, *Biochim. Biophys. Acta 1456*, 56−66.
47. Pecoraro, C., Gennis, R. B., Vygodina, T. V., and Konstantinov, A. A. (2001) Role of the K-channel in the pH-dependence of the reaction of cytochrome *c* oxidase with hydrogen peroxide, *Biochemistry 40*, 9695−9708.
48. Watmough, N. J., Cheesman, M. R., Greenwood, C., and Thomson, A. J. (1994) Cytochrome *bo* from *Escherichia coli*: Reaction of the oxidized enzyme with hydrogen peroxide, *Biochem. J. 300*, 469−475.
49. Brittain, T., Little, R. H., Greenwood, C., and Watmough, N. J. (1996) The reaction of *Escherichia coli* cytochrome *bo* with H_2O_2: Evidence for the formation of an oxyferryl species by two distinct routes, *FEBS Lett. 399*, 21−25.
50. Moody, A. J. and Rich, P. R. (1994) The reaction of hydrogen peroxide with pulsed cytochrome *bo* from *Escherichia coli*, *Eur. J. Biochem. 226*, 731−737.
51. Vygodina, T. V., and Konstantinov, A. A. (1988) H_2O_2-induced conversion of cytochrome *c* oxidase peroxy complex to oxoferryl state, *Ann. NY Acad. Sci. 550*, 124−138.
52. Gorren, A. C. F., Dekker, H., and Wever, R. (1986) Kinetic investigations of cytochrome *c* oxidase with hydrogen peroxide, *Biochim. Biophys. Acta 852*, 1−92.
53. Weng, L., and Baker, G. M. (1991) Reaction of hydrogen peroxide with the rapid form of resting cytochrome oxidase, *Biochemistry 30*, 5727−5733.
54. Vygodina, T., and Konstantinov, A. (1989) Effect of pH on the spectrum of cytochrome *c* oxidase hydrogen peroxide complex, *Biochim. Biophys. Acta 973*, 390−398.
55. Fabian, M., and Palmer, G. (2001) Proton involvement in the transition from the "peroxy" to the ferryl intermediate of cytochrome *c* oxidase, *Biochemistry 40*, 1867−1874.
56. Babcock, G. T., and Wikström, M. (1992) Oxygen activation and the conservation of energy in cell respiration, *Nature 356*, 301−309.
57. Riistama, S., Hummer, G., Puustinen, A., Dyer, R. B., Woodruff, W. H., and Wikström, M. (1997) Role of water in the proton translocation mechanism of the haem-copper oxidases, *FEBS Lett. 414*, 275−280.
58. Hofacker, I., and Schulten, K. (1998) Oxygen and proton pathways in cytochrome *c* oxidase, *Proteins 30*, 100−107.
59. Pomes, R., Hummer, G., and Wikström, M. (1998) Structure and dynamics of a proton shuttle in cytochrome *c* oxidase, *Biochim. Biophys. Acta 1365*, 255−260.
60. Olsson, M. H. M., Sharma, P. K., and Warshel, A. (2005) Simulating redox coupled proton transfer in cytochrome *c* oxidase: Looking for the proton bottleneck, *FEBS Lett. 579*, 2026−2034.
61. Verkhovskaya, M. L., García-Horsman, A., Puustinen, A., Rigaud, J. L., Morgan, J. E., Verkhovsky, M. I., and Wikström, M. (1997) Glutamic acid 286 in subunit I of cytochrome bo_3 is involved in proton translocation, *Proc. Natl. Acad. Sci. U.S.A. 94*, 10128−10131.
62. Smirnova, I., Ädelroth, P., Gennis, R. B., and Brzezinski, P. (1999) Aspartate-132 in cytochrome *c* oxidase from *Rhodobacter sphaeroides* is involved in a two-step proton transfer during oxo-ferryl formation, *Biochemistry 38*, 6826−6833.
63. Ostermeier, C., Harrenga, A., Ermler, U., and Michel, H. (1997) Structure at 2.7 Å resolution of the *Paracoccus denitrificans* two-subunit cytochrome *c* oxidase complexed with an antibody F_v fragment, *Proc. Natl. Acad. Sci. U.S.A. 94*, 10547−10553.
64. Humphrey, W., Dalke, A., and Schulten, K. (1996) VMD: Visual molecular dynamics, *J. Mol. Graph. 14*, 33.

BI0511336